Journal of Membrane Science 749 (2026) 125409

Contents lists available at ScienceDirect

Journal of Membrane Science

journal homepage: www.elsevier.com/locate/memsci

Near-ambient temperature synthesis of NaA zeolite membranes towards high-efficiency ethanol dehydration pervaporation and ammonia separation

Yunlei Gao [a], Meng Ge [a,*], Siqi Tao [a], Yi Liu [a], Shengyan Meng [a], Kunpeng Yu [a], Jiahui Yan [a], Mingming Wu [a], Kaishi Ding [a], Xinyu He [a], Wenwen Dong [a], Yi Liu [a,b,**]

[a] State Key Laboratory of Fine Chemicals, Frontiers Science Center for Smart Materials, School of Chemical Engineering, Dalian University of Technology, Dalian, 116024, China

[b] Dalian Key Laboratory of Membrane Materials and Membrane Processes, Dalian University of Technology, Dalian, 116024, China

ARTICLE INFO

Keywords:
NaA zeolites
Membranes
Pervaporation
Near-ambient temperature synthesis
Ammonia separation

ABSTRACT

NaA zeolite membranes are typically synthesized via hydrothermal growth, which requires elevated temperatures and autogenous pressure, raising significant concerns regarding energy efficiency and safety. In this study, we report a near-ambient temperature synthetic protocol that dramatically lowers energy input and safety risks. Among various synthetic factors, employing a low-concentration precursor solution was proven to play a critical role, since not only excessive nucleation in the bulk solution could be suppressed but also undesired phase transition could be avoided, facilitating the formation of uniform and well-intergrown NaA zeolite membrane during near-ambient temperature epitaxial growth. Besides high crystallinity, HRTEM reveals that there is not only dense intercrystalline boundaries between neighboring crystallites but also compact intracrystalline dislocations within individual crystallites, demonstrating the presence of few non-selective defects in the membrane. Ethanol dehydration pervaporation experiments indicated that NaA zeolite membranes synthesized under optimized conditions exhibited water/ethanol separation factor of ∼3700 with total flux of 2.4 kg m^{-2} h^{-1} at 348 K. Furthermore, gas permeation results revealed that our membrane exhibited NH_3/H_2 and NH_3/N_2 separation factor of 17.6 and 26.7 with NH_3 permeance of 1.2×10^{-7} mol m^{-2} s^{-1} Pa^{-1}, demonstrating great promise for energy-efficient NH_3 recovery during Haber-Bosch process.

1. Introduction

NaA zeolite membranes have shown great promise in high-efficiency pervaporation dehydration of organics, owing to their intrinsic hydrophilicity, appropriate pore size, and framework robustness [1]. Various methods, including hydrothermal synthesis [2–4], microwave heating [5], and sol-gel processing [6,7], have been employed for fabricating high-performance NaA zeolite membranes. Nonetheless, the above protocols typically rely on elevated reaction temperatures and autogenous pressures, posing safety hazards and incurring high energy costs [8]. Therefore, the development of synthetic strategies that ensure energy saving and operational safety without compromising performance is highly desirable.

Lowering reaction temperature has emerged as an effective strategy to overcome the limitations encountered in common hydrothermal synthesis. Reduced thermal input effectively slows down the overall reaction rate, which in turn enables more precise and favorable control over the nucleation and growth kinetics of zeolite crystals, facilitating the production of uniform membranes with fewer non-selective defects [8–13]. However, simply temperature reduction may be insufficient for overcoming the nucleation barrier of NaA zeolite crystallites on the substrate surface. Previous studies revealed that zeolite crystallization fundamentally involved hydrolysis of silicoaluminate precursors to generate metastable $[SiO_4]^{4-}$ or $[AlO_4]^{5-}$ hydroxyl tetrahedra, followed by their condensation into stable zeolitic frameworks through oxygen-bridged covalent bonds [14–16]. The topological configuration

---

* Corresponding author.

** Corresponding author. State Key Laboratory of Fine Chemicals, Frontiers Science Center for Smart Materials, School of Chemical Engineering, Dalian University of Technology, Dalian, 116024, China.

E-mail addresses: gemeng@dlut.edu.cn (M. Ge), diligenliu@dlut.edu.cn (Y. Liu).

https://doi.org/10.1016/j.memsci.2026.125409
Received 18 January 2026; Received in revised form 5 March 2026; Accepted 18 March 2026

of zeolites is dictated by both supramolecular assembly dynamics during precursor condensation and PH-dependent speciation of reactive Si/Al ratio (SAO) species in the reaction medium. Therefore, poorly optimized synthetic conditions may cause insufficient driving force for epitaxial growth, premature bulk crystallization, and even crystal transformation, leading to the formation of NaA zeolite membranes with undesirable microstructure, and therefore, inferior separation performance.

It should be noted that, reducing energy input at the expense of extending reaction duration remains technically and economically attractive under certain conditions. Aiming at addressing high energy consumption and safety concerns during membrane processing, in this study, we developed a near-ambient temperature process for synthesizing NaA zeolite membranes from diluted precursor solutions (Fig. 1) [9,17,18]. Simultaneously, a series of advanced electron microscopy techniques, including HRTEM, HAADF-STEM and EDS, are employed to directly resolve the nanoscale structural features of NaA zeolite membranes. Beyond high crystallinity, HRTEM reveals the presence of both dense intercrystalline boundaries and compact intracrystalline dislocations, demonstrating the presence of few non-selective defects in the membrane. Ethanol dehydration pervaporation experiments revealed that as-prepared membrane exhibited H_2O/EtOH separation factor (SF) exceeding 3700 with water flux of 2.4 kg m^{-2} h^{-1} at 348 K, which was comparable with other high-performance NaA zeolite membranes reported in the literature. Aiming at energy-efficient NH_3 recovery during Haber-Bosch process, $NH_3/H_2/N_2$ separation performance of obtained NaA zeolite membrane was evaluated further. Experimental results revealed that our membrane exhibited NH_3/H_2 and NH_3/N_2 separation factor of 17.6 and 26.7 with NH_3 permeance of 1.2×10^{-7} mol m^{-2} s^{-1} Pa^{-1}.

2. Experimental

2.1. Reagents and materials

Sodium aluminate ($NaAlO_2$, AR), tetramethylammonium hydroxide (TMAOH, 25 wt%), sodium hydroxide (NaOH, AR), silica sol (SiO_2, 40 wt%), and aluminum isopropoxide ($Al(O\text{-}iPr)_3$, 98 wt%) were used as received. Porous α-Al_2O_3 tubes (5 cm length, 70 nm pore size, 12 mm outer diameter, and 8 mm inner diameter) were used as received.

2.2. Preparation of NaA zeolite seeds and NaA zeolite seeds suspension

NaA zeolite seeds were synthesized with slight modification based on a previous protocol [19]. Initially, 0.13 g NaOH was dissolved in 17 ml DI water, followed by addition of 16 ml TMAOH aqueous solution. The above solution was heated in a water bath and maintained at 60 °C. Subsequently, 2.08 g $Al(O\text{-}iPr)_3$ was added to this solution, followed by vigorous stirring until complete dissolution. After cooling, 3 g silica was added dropwise and aged for 10 h. Finally, the above solution was placed in a rotating oven and reacted at 100 °C for 12 h.

A 0.5 wt% NaA seed suspension was prepared using the seeds synthesized as described in Section 1.2. To enhance the adhesion between the support and the seed layer, a 0.1 wt% hydroxypropyl cellulose (HPC) solution was added into the seed suspension. Specifically, 50 g deionized water was heated to 80 °C, followed by addition of 1 g HPC to obtain a 0.2 wt% HPC solution. The mixture was stirred vigorously in an 80 °C water bath until the polymer was completely dissolved. Subsequently, 0.25 g NaA zeolite seeds was mixed with 25 g of deionized water and 25 g 0.2 wt% HPC solution, followed by stirring at ambient temperature for 7 days to ensure the formation of monodispersed NaA zeolite seed dispersion (Fig. S1). Detailed procedure for the preparation of NaA zeolite seed suspension was schematically illustrated in Fig. S2.

2.3. Preparation of NaA zeolite membranes

The precursor solution composition and reaction duration for the synthesis of NaA zeolite membranes are listed in Table S1. For convenience, NaA zeolite membranes synthesized under different reaction conditions were named as M1-M9, respectively. For instance, in terms of M1, solution A was prepared by dissolving 5 g NaOH and 0.42 g $NaAlO_2$ in 25 g DI water, while solution B was prepared by sequentially dissolving 5 g NaOH and 1.36 g SiO_2 into 25 g DI water. Then solution B was dropwise to solution A, followed by aging at room temperature for 10 h. Finally, the seeded substrate was placed vertically in an oven at 30 °C. After 3 days of reaction, the resulting membrane was removed and rinsed thoroughly with deionized water prior to use.

2.4. Ethanol dehydration pervaporation test

Ethanol dehydration pervaporation performances of NaA zeolite membranes were evaluated under different conditions. The apparatus used for pervaporation experiments was illustrated in Fig. S3. The membrane model was heated in a thermostatic water bath and evacuated with a vacuum pump during pervaporation test. Two cold traps filled with liquid N_2 were used to collect the permeate solution. The composition of solutions obtained from both feed and permeate sides was analyzed by gas chromatogram (Agilent 8860 GC).

The total flux (J) and SF (α) for pervaporation are defined by Equations (1) and (2), respectively:

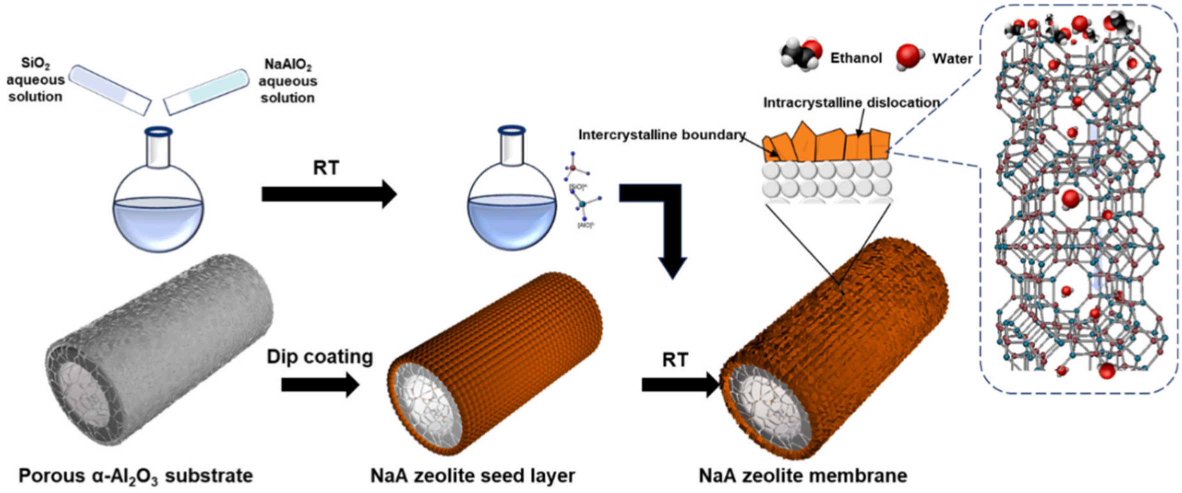

Fig. 1. Schematic illustration of near-ambient temperature epitaxial growth of NaA zeolite membranes.

$$J = \frac{W}{\Delta t A} \tag{1}$$

$$\alpha_{i/j} = \frac{x_{ip}}{x_{if}} \frac{x_{jf}}{x_{jp}} \tag{2}$$

where W is the total weight of the permeate (kg), Δt is the collecting time (h), A is the membrane area, x_{ip} is the weight fraction of species i at the permeate side, and x_{if} is the weight fraction of species i at the feed side [6,20–22].

2.5. Characterization

The morphology of the NaA zeolite membrane was characterized using a Schottky field-emission scanning electron microscope (Hitachi FlexSEM SU5000) operated at an acceleration voltage of 10 kV. The morphology of NaA zeolite membrane was characterized using Schottky

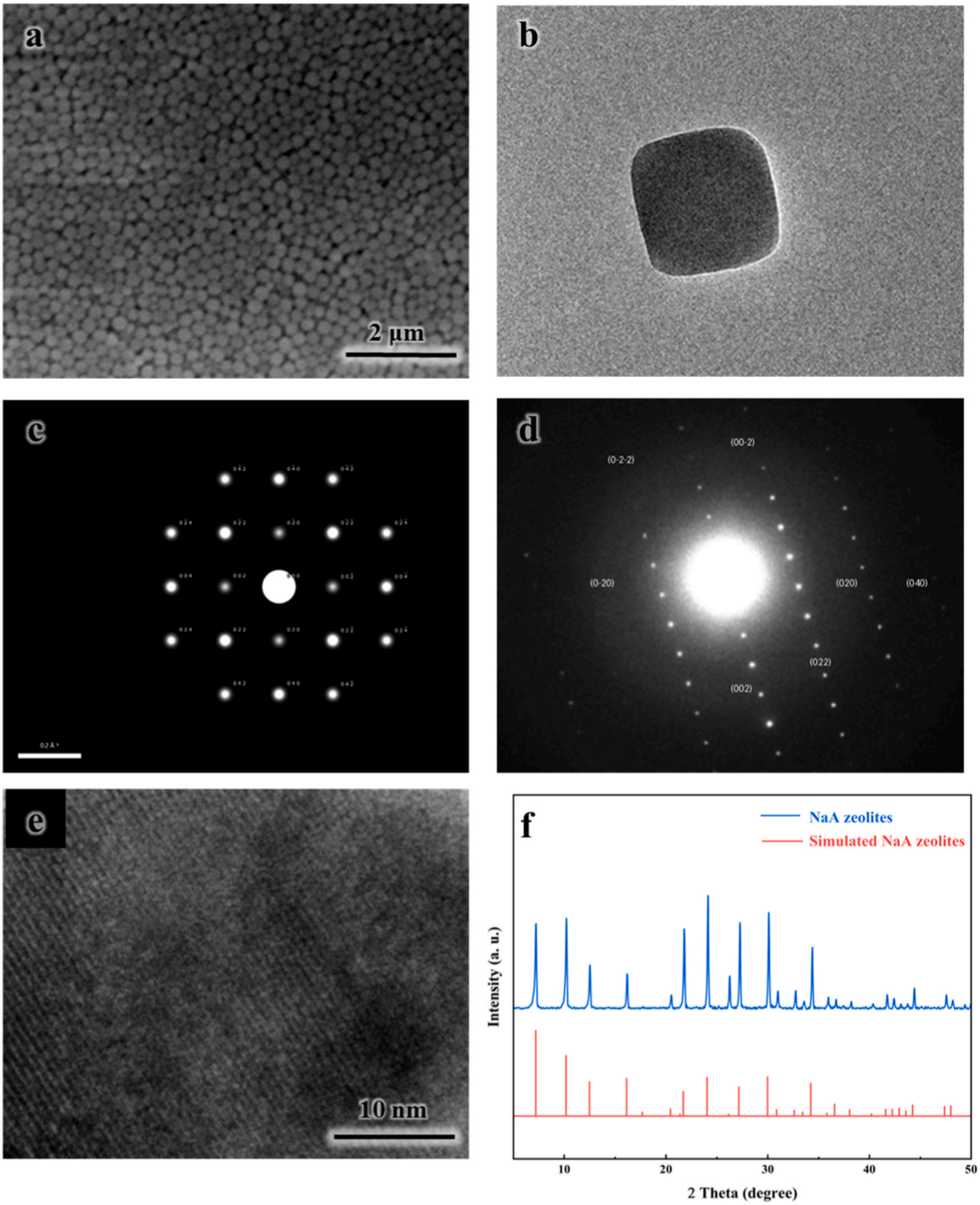

Fig. 2. (a) SEM image of NaA zeolite seeds, (b) low-magnification TEM image of NaA zeolite seeds, (c) simulated SAED pattern of the LTA framework along the [100] zone axis, (d) SAED pattern of the prepared LTA single crystal with all diffraction spots indexed and corresponding (hkl) planes indicated, (e) HRTEM image of NaA zeolite seeds, and (f) XRD patterns of NaA zeolite seeds (blue) and simulated NaA zeolites from PDF#39-0223 (red). (For interpretation of the references to colour in this figure legend, the reader is referred to the Web version of this article.)

Scanning Electron Microscope (Hitachi FlexSEM, SU5000) with an acceleration voltage of 10 KV. HAADF-STEM and HRTEM images were obtained on Field Emission Transmission Electron Microscope (JEOL JEM-F200). Prior to testing, the cross-sectional sample was thinned using Focused Ion Beam (Helios G4 UX). The crystal structure of prepared samples was analyzed using an X-ray diffractometer (Rigaku Smartlab) with a Cu Kα radiation source. The scanning rate was 8° min^{-1}, the scanning step size was 0.02°, the scanning angle was 5-50°, the scanning voltage was 45 kV, and the current was 200 mA. N_2 adsorption-desorption isotherms at 77 K were measured using a Micromeritics ASAP 2020 Plus gas adsorption analyser. Prior to measurement, the samples were outgassed at 300 °C for 12 h. Total surface area was derived from the BET model, micropore volume and micropore surface area were determined from the t-plot method, and total pore volume was measured at $P/P_0 = 0.995$ as a single point.

3. Results and discussion

3.1. Synthesis of NaA zeolite seeds

NaA zeolite seeds were synthesized according to a modified literature method. As shown in Fig. 2a, the seeds synthesized under optimized reaction conditions exhibited uniform cubic morphology with an average size of ~200 nm. TEM combined with SAED was further employed to investigate structural characteristics of NaA zeolite seeds. As shown in Fig. 2b, low-magnification TEM image revealed that the seeds exhibited uniform cubic morphology with smooth surface and well-defined edge, indicating high morphological homogeneity. Corresponding SAED patterns (Fig. 2c and d) exhibited sharp and symmetrically arranged diffraction spots without any diffuse halos, which was indicative of the formation of single-crystalline NaA zeolite structure as well as the absence of amorphous or impure phase. Corresponding HRTEM image (Fig. 2e) displayed distinct lattice fringes, further corroborating the high crystallinity. The above results convincingly demonstrated that obtained NaA zeolite seeds possessed excellent crystallinity, high phase purity, and uniform morphology. In addition, relevant XRD pattern was found to be consistent with the standard XRD pattern of NaA zeolites, confirming that obtained powders belonged to pure NaA zeolite phase (Fig. 2f) [23,24]. Such structural perfection is essential for subsequent membrane fabrication, as uniform and well-crystallized seeds have been proven to be advantageous for the formation of uniform and well-intergrown zeolite membranes. Simultaneously, N_2 adsorption measurements revealed a BET surface area of 456.56 $m^2\ g^{-1}$ with total pore volume of 0.402 $cm^3\ g^{-1}$ (Figs. S4 and S5), which was comparable with other NaA zeolites reported in the literature [19,23]. In addition, the TG curve of as-prepared NaA zeolites (Fig. S6) exhibited no significant weight loss below 600 °C, demonstrating excellent thermal stability at elevated temperatures.

3.2. Preparation of NaA zeolite membrane

Subsequently, the seed layer was deposited on tubular α-Al_2O_3 substrate through dip-coating. As illustrated in Fig. 3a, under optimized conditions, NaA zeolite seeds were uniformly deposited on the support surface, resulting in the formation of continuous seed layer. The corresponding cross-sectional view (Fig. 3b) revealed that its thickness reached 200-300 nm. Obviously, homogeneous coverage of NaA zeolite seeds on the substrate surface was beneficial for the formation of uniform and well-intergrown NaA zeolite membrane.

In the next step, epitaxial growth was carried out to seal the open space in the seed layer. As shown in Fig. 3c and d, after reaction for 20 days, a well-intergrown NaA zeolite membrane with thickness of 4.2 μm was readily formed. Notably the mother liquor remained transparent, suggesting that the near-ambient temperature condition effectively suppressed bulk nucleation, thereby facilitating the full utilization of reactants for membrane growth [8].

It should be noted that in comparison with previous studies (Table 1), adoption of diluted aqueous precursor solution was indispensable for obtaining NaA zeolite membranes with desired microstructure. In parallel, we further tried near-ambient temperature synthesizing NaA zeolite membranes from more concentrated precursor solutions with recipes following reported literatures [3,5,24–33]. Experimental results of M10-M15 in Table S2 indicated all obtained membranes were non-continuous and non-uniform; simultaneously, all bulk solutions became turbid. We therefore inferred that employing diluted precursor solution facilitated suppression of bulk nucleation in the precursor solution with no compromise in membrane continuity under ambient conditions (Fig. S7).

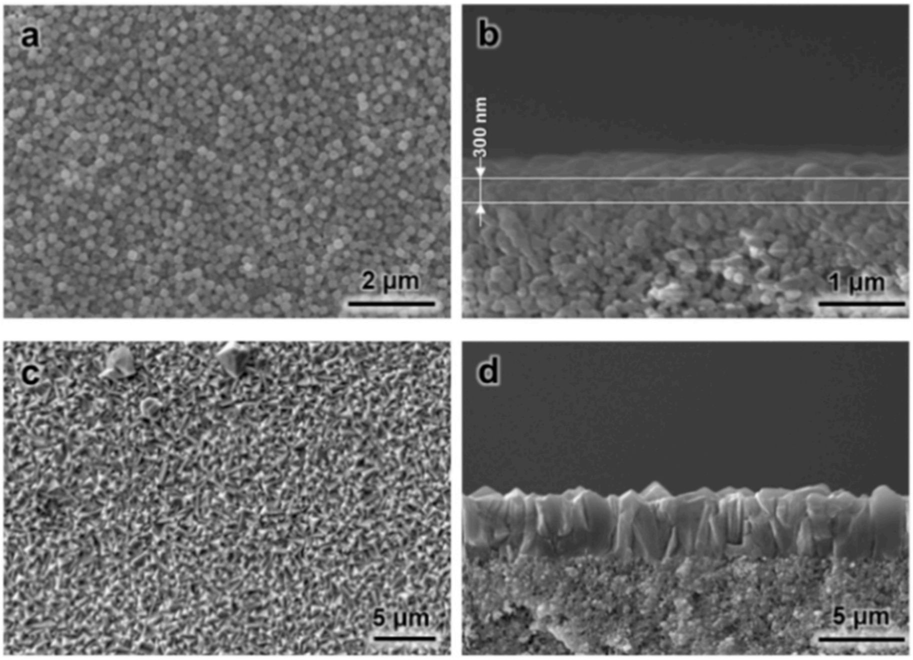

Fig. 3. SEM images of (a, b) NaA zeolite seed layer and (c, d) NaA zeolite membrane after near-ambient temperature epitaxial growth for 20 days.

Table 1
Comparison of precursor solution composition and reaction temperature of NaA zeolite membranes with previous literature.

Precursor solution molar composition		Temperature	Reference
H_2O/Al_2O_3	H_2O/SiO_2		
240	120	100 °C	[25]
150	75	100 °C	[26]
120	60	80-120 °C	[27]
1000	200	80 °C	[24,28–30,34]
273	152	90 °C	[31]
500-1000	200-250	80 °C	[32,33]
1200	**333**	**30 °C**	**This work**

To identify the formation stages of NaA zeolite membranes during RT epitaxial growth, the morphology and crystallinity of membranes synthesized at different reaction durations were examined. At the initial stage, only a discrete layer of zeolite crystallites was coated on the substrate surface (Fig. 4a and b). Corresponding XRD pattern (Fig. S8a) revealed merely weak diffraction peaks derived from the seed layer, indicating that the crystallization process scarcely occurred. Prolonging the reaction duration to 15 days led to progressive coalescence of NaA zeolite crystallites accompanying with their morphological transformation from monodispersed particles into interconnected crystalline domains (Fig. 4c). Relevant XRD patterns exhibited characteristic reflections at 2θ values of 7.2°, 10.2°, 12.4°, 16.1°, 21.6°, 24.0° and 27.0°, which could be assigned to (200), (220), (222), (420), (440), (622) and (642) planes of NaA zeolite phase, respectively (Fig. S8a). Obviously, gradual sharpening and intensity enhancement of above peaks confirmed increased crystallinity and continuity of NaA zeolite membranes. Further extending the reaction duration to >20 days led to effective elimination of grain boundary defects and therefore, formation of well-intergrown membranes (Fig. 3c) [14,35]; simultaneously, XRD patterns at this stage displayed sharp and intense diffraction peaks belonging to pure NaA zeolite phase, demonstrating that NaA zeolite membranes with high crystallinity were readily obtained. However, further extending the reaction duration to 40 days led to the generation of substantial twin crystals on the membrane surface (Fig. 4d); simultaneously, relevant XRD pattern revealed that not only the relative intensity of diffraction peaks belonging to NaA zeolite phase was remarkably enhanced but also the unidentified impure phase was present, which may negatively influence pervaporation and gas separation performances of NaA zeolite membranes as convinced in previous literature [36]. Therefore, maintaining epitaxial growth duration of ~20 days was optimum for synthesizing NaA zeolite membranes with optimized microstructure.

The microstructure evolution of NaA zeolite membranes with reaction duration can be rationalized through considering the interplay between reactant concentration and nucleation kinetics in the precursor solution. Since the reactant concentration in the precursor solution remained below the threshold for NaA zeolite nucleation in the precursor solution, during epitaxial growth, heterogenous nucleation of NaA zeolites in the bulk solution was effectively suppressed, resulting in high-efficiency utilization of nutrients in the bulk solution for patching non-selective grain boundary defects in the membrane [37]. Nonetheless, further prolonging reaction duration may lead to excessive nucleation in the bulk solution, and therefore, excessive nutrient consumption during epitaxial growth. As a result, insufficient supply of nutrients occurred, causing the formation of NaA zeolite membranes with both comprised uniformity and continuity [34].

Besides reactant concentration, another factor influencing the microstructure of NaA zeolite membranes represents the NaOH concentration of precursor solution [38]. Herein the NaOH concentration is reflected by molar ratio of H_2O/Na_2O, which simultaneously regulates hydroxide activity and charge-balancing cation concentration in the aluminosilicate system. It is well-recognized that increasing alkalinity favors crystal phase transition from thermodynamically metastable NaA zeolites to more thermodynamically stable SOD or FAU zeolites [39]. In contrast, relatively mild alkalinity of the precursor solution may not only ensure phase stability of NaA zeolites but also suppress undesirable crystal transformation, resulting in final formation of pure-phase NaA zeolite membranes [38]. To verify the effect of sodium hydroxide concentration of the precursor solution on their microstructures, NaA zeolite membranes were further synthesized with varying H_2O/Na_2O ratio. It was found that well-intergrown NaA zeolite membrane could be prepared upon maintaining a H_2O/Na_2O ratio of 24 (Fig. 3c). In contrast, increasing the H_2O/Na_2O ratio to 48 and 96 led to incomplete hydrolysis of SiO_2 and $NaAlO_2$ reactants, resulting in the formation of non-continuous NaA zeolite membranes [40] (Fig. 4e and f). However, decreasing the H_2O/Na_2O ratio to 16 or lower triggered not only complete dissolution of the seed layer as evidenced by the XRD pattern (Fig. S8b) but also the formation of impure FAU crystallites (Fig. 4g and h) in the membrane [41]. This could be attributed to the dependence of saturation degree of hydrolyzed SiO_2 and $NaAlO_2$ reactants on the alkalinity, which in turn regulated the concentration of soluble silicate and aluminate species in the precursor solution [40]. Therefore, maintaining appropriate concentration of NaOH of the precursor solution was of vital importance for obtaining pure-phase NaA zeolite membranes with optimized microstructure.

3.3. Pervaporation and gas separation tests

Finally, ethanol dehydration pervaporation performance of obtained NaA zeolite membranes was evaluated. And the pervaporation performance is shown in Table S3. It is worth noting that all other unlisted NaA zeolite membranes mentioned in this paper exhibited liquid leakage during the pervaporation performance tests, so their performance was not included in the table. This is consistent with the observation of large areas of bare support under the electron microscope. Experimental results indicated that M4 exhibited water/ethanol SF of ~3700 with water flux of 2.4 kg $m^{-2}h^{-1}$ at 348 K; moreover, its performance was unchanged during continuous operation at 348K for over 100 h, which was indicative of intrinsic framework robustness in aqueous environments.

We further investigated the influence of operation temperature on the water/ethanol pervaporation dehydration performance. As shown in Table 2, upon increasing the operation temperature from 323 to 363 K, the permeate flux significantly increased from 0.92 to 4.12 kg m^{-2} h^{-1}, while the separation factor (SF) decreased from 3856 to 3157. This trade-off behavior can be interpreted based on the solution–diffusion mechanism [42]. Increasing temperature enhances molecular mobility and thus increases the diffusion coefficients of both water and ethanol in NaA zeolite channels, resulting in higher permeation flux. However, as temperature rises, the adsorption affinity of water towards the zeolite framework decreases significantly, weakening its preferential sorption over ethanol. Consequently, although both components permeate faster at elevated temperature, the reduction in water sorption selectivity leads to a noticeable decline in SF. Therefore, the apparent activation energy derived from the Arrhenius plots (Fig. S9) reflects the combined contributions of diffusion activation energy and sorption enthalpy, rather than representing intrinsic diffusion resistance alone. The lower apparent activation energy of water compared with ethanol is mainly attributed to its stronger sorption interaction with the hydrophilic NaA framework, which diminishes with increasing temperature, leading to reduced separation performance. It should be noted that similar behavior has been well reported in previous literature [43].

Besides pervaporation, considering intrinsic framework polarity and the presence of hydroxyl groups in NaA zeolite membranes, its $NH_3/H_2/N_2$ separation performance was evaluated further. Gas permeation results revealed that our membrane exhibited NH_3/H_2 and NH_3/N_2 SF of 17.6 and 26.7 with NH_3 permeance of 1.2×10^{-7} mol m^{-2} s^{-1} Pa^{-1} (Fig. S10) with the apparatus illustrated in Fig. S11. While the NH_3 separation performance reported in this study does not surpass the best

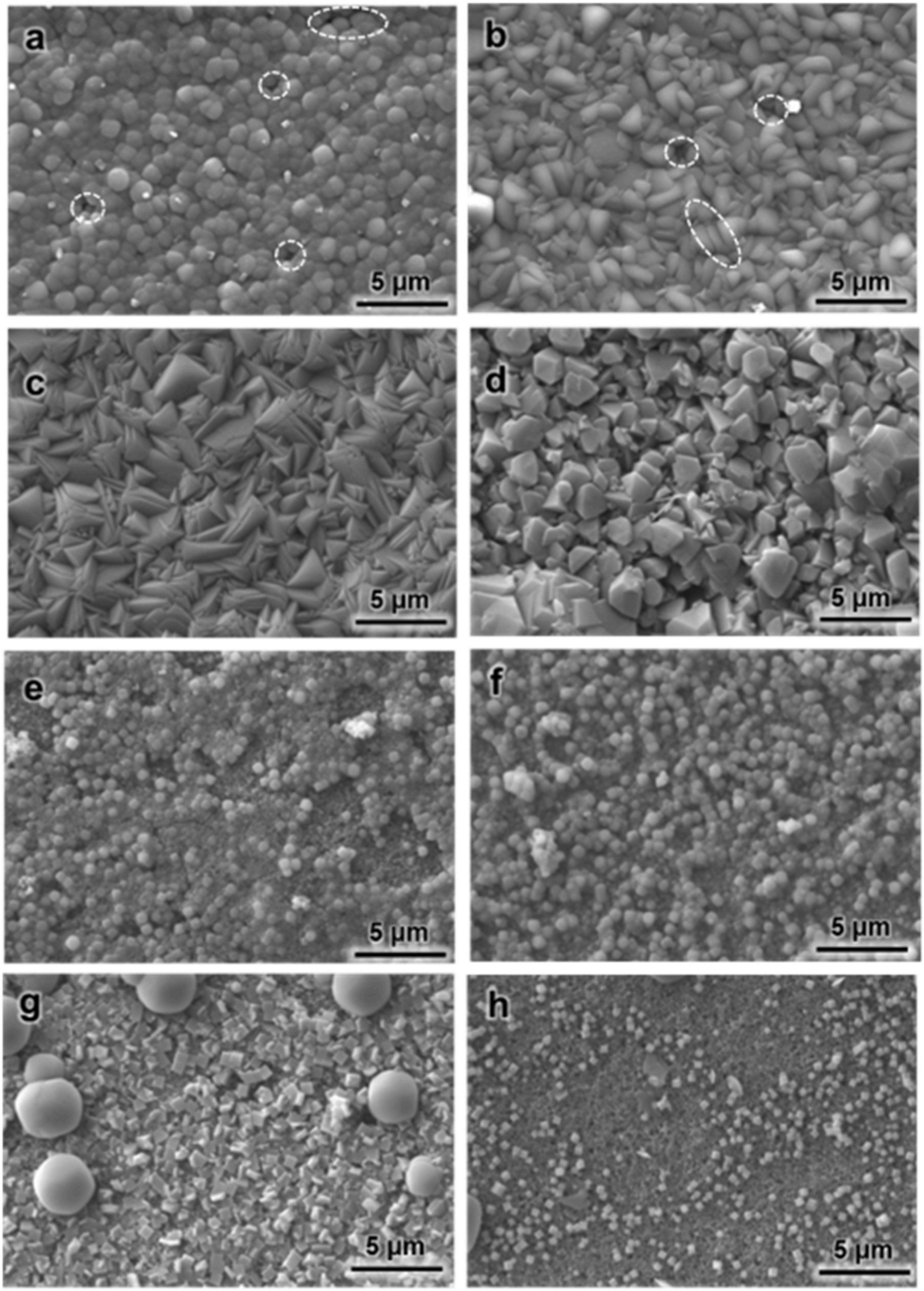

Fig. 4. SEM images of NaA zeolite membranes synthesized at near-ambient temperature for (a) 3 days (M1), (b) 7 days (M2), (c) 15 days (M3) and (d) 40 days (M5). The white dashed circles in (a) and (b) indicate surface defects observed at reduced reaction duration. SEM images of NaA zeolite membranes synthesized with H_2O/Na_2O ratios of (e) 96 (M6), (f) 48 (M7), (g) 16 (M8) and (h) 12 (M9).

Table 2
Ethanol dehydration pervaporation performance of NaA zeolite membrane at varying operation temperature.

Temperature (K)	Water flux (kg·m^{-2}·h^{-1})	Water/ethanol SF
323	0.9	3856
333	1.4	3798
343	1.9	3778
348	2.4	3722
353	3.1	3304
363	4.1	3157

literature values [44], this study constitutes the first report on NH_3 permselective behaviour of NaA zeolite membranes, offering valuable fundamental insights in membrane-based NH_3 separation.

To further assess the competitiveness of the present membrane, its pervaporation performance was compared with previously reported NaA zeolite membranes (Table S4). Although the separation performance is slightly lower than those of best-performing NaA zeolite membranes, it remains within the typical range reported for NaA zeolite membranes. Nevertheless, the present strategy significantly simplifies the fabrication procedure and avoids high-temperature treatment, thereby reducing energy consumption, operational complexity, and safety risks.

Previous studies revealed that the grain boundary structure in zeolite membranes played an important role in modulating their separation performances, yet direct atomic-resolution of their grain boundaries has remained elusive [14,45]. In this study, we present detailed structural analysis with SEM, TEM and HAADF-STEM for elucidating the fine structure of grain boundary regions.

SEM imaging of FIB-prepared cross-sectional specimens provides direct evidence for the existence of a distinct grain boundary phase (GBP) of inter-crystalline defects [46]. Linear bright contrasts are clearly observed at the interfaces between adjacent crystallites (Fig. 5a and b), and these features indicate regions of higher projected density. Considering that the contrast is strongly correlated with atomic number and mass-thickness contributions, the enhanced brightness at grain boundaries suggests the formation of a dense non-zeolitic phase within grain boundary regions.

We further conducted HRTEM characterization to clarify the structural nature of above grain boundaries. As shown in c and d, a uniform band of approximately 5 nm in width is consistently detected between adjacent well-crystallized NaA zeolite crystallites. This region exhibits a darker contrast compared with the NaA zeolite lattice, while the lack of long-range ordering, combined with the darker projected contrast, confirms that the GBP corresponds to an amorphous phase, rather than crystalline or defect-modified NaA zeolite structure. The sharp structural discontinuity between the amorphous band and the adjacent zeolite lattices further convinces the presence of a chemically and structurally distinct intergranular layer.

HRTEM observations further provide direct evidence of intracrystalline lattice distortions within individual NaA zeolite crystallites. As shown in Fig. 6a, the d_{200} lattice fringes exhibit pronounced bending and curvature in localized regions. Such deviations from linear periodicity indicate the presence of dislocation-induced strain fields, a common signature of intracrystalline defects in aluminosilicate frameworks [47,48]. Further structural complexity is observed in Fig. 6b, where the same crystallite displays both d_{200} and d_{222} lattice fringes in close spatial proximity. Rather than representing two overlapping grains, the fringes remain crystal graphically continuous, suggesting that the crystal is oriented near a mixed-zone axis in which both planes approach imaging conditions simultaneously. The intersection of two lattice spacings within the same coherent domain reflects a localized tilt or rotation of the crystal lattice. Such coexisting fringe orientations are well-known in cubic frameworks in cases where slight deviations from high-symmetry

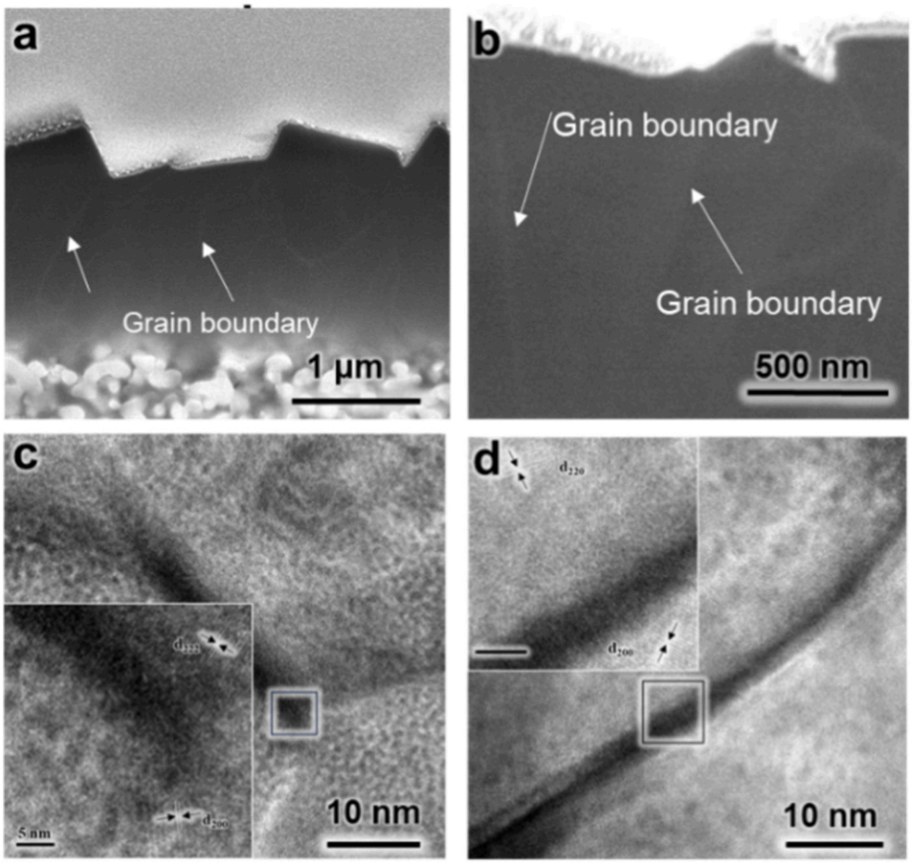

Fig. 5. STEM images of (a, b) M4 synthesized from FIB lamella and (c, d) HRTEM images of the GBP in NaA zeolite membrane.

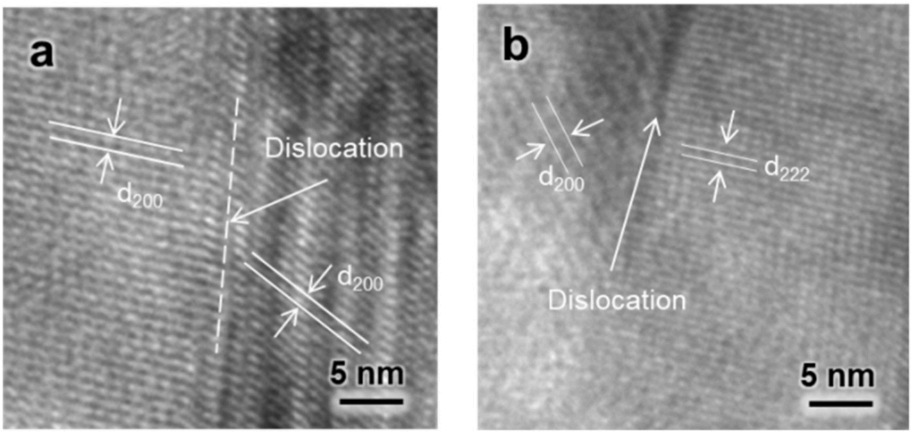

Fig. 6. HRTEM images of intracrystalline defects in M4: (a) lattice curvature associated with dislocation strain field; (b) localized lattice distortion with slight angular deviation within a single crystallite.

zone axes allow multiple plane families to be resolved concurrently under HRTEM.

It is well recognized that intracrystalline dislocations and local orientation gradients are intrinsic to NaA zeolite crystallites within the membrane. Above structures may arise from local variations in growth-front alignment, stress accommodation during crystallite coalescence, and nano-scale compositional fluctuations inherited from the synthesis environment [49]. Such intracrystalline distortions are not expected to create non-zeolitic leakage pathways; alternatively, local bending or rotation of the LTA lattice may introduce slight variations in channel alignment and tortuosity, potentially increasing the diffusional path length and thereby imposing a modest resistance to flux. Simultaneously, because these distortions remain confined within the crystalline framework and do not generate open defects, they are unlikely to compromise the intrinsic molecular sieving function of NaA zeolites. Therefore, while intracrystalline dislocations are inherent structural features of NaA zeolite membranes, their contribution to membrane selectivity is expected to be quite limited.

To sum up, although both intercrystalline boundaries and intracrystalline dislocations were observed in NaA zeolite membranes [50], they may exert negligible impact on water/ethanol and $NH_3/H_2/N_2$ selectivity [38].

4. Conclusions

In this study, we established an energy-efficient and safe near-ambient temperature epitaxial approach for synthesizing NaA zeolite membranes from diluted precursor solutions. Advanced electron microscopy confirmed that although dense intercrystallite boundaries and compact intracrystalline dislocations were present in the membrane, they did not create non-selective permeation pathways. Synthesized NaA zeolite membrane exhibited steady water/ethanol SF of ~3700 with water flux of 2.4 kg m^{-2} h^{-1} at 348 K during ethanol dehydration pervaporation test, which was comparable with other high-performance NaA zeolite membranes. $NH_3/H_2/N_2$ separation test further revealed a pronounced preferential permeation of NH_3 over H_2 (17.6) and N_2 (26.7), further indicating the presence of few non-selective defects in the membrane. The near-ambient temperature synthetic route provides an energy-efficient and safer alternative to conventional hydrothermal synthesis, thus holding great promise for scalable applications.

CRediT authorship contribution statement

Yunlei Gao: Writing – original draft, Methodology, Investigation, Formal analysis, Data curation, Conceptualization. **Meng Ge:** Writing – review & editing, Supervision, Formal analysis. **Siqi Tao:** Investigation, Data curation. **Yi Liu:** Writing – review & editing, Supervision, Resources, Methodology, Funding acquisition, Conceptualization. **Shengyan Meng:** Formal analysis. **Kunpeng Yu:** Methodology. **Jiahui Yan:** Methodology. **Mingming Wu:** Supervision. **Kaishi Ding:** Investigation. **Xinyu He:** Investigation. **Wenwen Dong:** Data curation. **Yi Liu:** Methodology, Data curation.

Declaration of competing interest

The authors declare that they have no known competing financial interests or personal relationships that could have appeared to influence the work reported in this paper.

Acknowledgements

The authors are grateful to National Natural Science Foundation of China (22478056 and 22578043), National Key Research and Development Program of China (2023YFB3810700), Liaoning Province Funds for Distinguished Young Scholars (2024JH3/50100002), State Key Laboratory of Catalysis (2024SKL-A-003), Science and Technology Innovation Fund of Dalian (2024JJ12GX027), and Fundamental Research Funds for the Central Universities (DUT22LAB602) for the financial support.

Appendix A. Supplementary data

Supplementary data to this article can be found online at https://doi.org/10.1016/j.memsci.2026.125409.

Data availability

The authors do not have permission to share data.

References

[1] D. Li, M. Ye, C. Ma, N. Li, Z. Gu, Z. Qiao, Preparation of a self-supported zeolite glass composite membrane for CO2/CH4 separation, Smart Mol 2 (3) (2024) e20240009, https://doi.org/10.1002/smo.20240009.

[2] S. Yamazaki, K. Tsutsumi, Synthesis of A-type zeolite membrane using a plate heater and its formation mechanism, Microporous Mesoporous Mater. 37 (1) (2000) 67–80, https://doi.org/10.1016/S1387-1811(99)00194-8.

[3] X. Xu, W. Yang, J. Liu, L. Lin, Synthesis of NaA zeolite membranes from clear solution, Microporous Mesoporous Mater. 43 (3) (2001) 299–311, https://doi.org/10.1016/S1387-1811(01)00209-8.

[4] G.J. Myatt, P.M. Budd, C. Price, S.W. Carr, Synthesis of a zeolite NaA membrane, J. Mater. Chem. 2 (10) (1992) 1103–1104, https://doi.org/10.1039/JM9920201103.

[5] X. Xu, W. Yang, J. Liu, L. Lin, Synthesis of NaA zeolite membrane by microwave heating, Sep. Purif. Technol. 25 (1) (2001) 241–249, https://doi.org/10.1016/S1383-5866(01)00108-3.

[6] H. Zhang, Y. Yang, Z. Wang, Synthesis of hierarchical LTA zeolite membranes by vapor phase transformation, J. Membr. Sci. 671 (2023) 121391, https://doi.org/10.1016/j.memsci.2023.121391.

[7] X. Xu, W. Yang, J. Liu, X. Chen, L. Lin, N. Stroh, H. Brunner, Synthesis and gas permeation properties of an NaA zeolite membrane, Chem. Commun. 7 (7) (2000) 603–604, https://doi.org/10.1039/B000478M.

[8] Y. Liu, S. Chen, T. Ji, J. Yan, K. Ding, S. Meng, J. Lu, Y. Liu, Room-temperature synthesis of zeolite membranes toward optimized microstructure and enhanced butane isomer separation performance, J. Am. Chem. Soc. 145 (14) (2023) 7718–7723, https://doi.org/10.1021/jacs.3c00009.

[9] M. Sen, K. Dana, N. Das, Development of LTA zeolite membrane from clay by sonication assisted method at room temperature for H(2)-CO(2) and CO(2)-CH(4) separation, Ultrason. Sonochem. 48 (2018) 299–310, https://doi.org/10.1016/j.ultsonch.2018.06.007.

[10] V.P. Valtchev, L. Tosheva, K.N. Bozhilov, Synthesis of zeolite nanocrystals at room temperature, Langmuir 21 (23) (2005) 10724–10729, https://doi.org/10.1021/la050323e.

[11] T. Xia, Y. Wu, T. Ji, W. Hu, K. Yu, X. He, B.H. Yin, Y. Liu, Mixed-matrix membranes incorporating hierarchical ZIF-8 towards enhanced CO2/N2 separation, Smart Mol 3 (2) (2025) e20240066, https://doi.org/10.1002/smo.20240066.

[12] P. Tong, T. Wu, M. Li, H. Wang, F. Zheng, L. Xu, W. Dou, Fluorescent probes for the visualization of membrane microdomain, deformation, and fusion, Smart Mol 3 (1) (2025) e20240059, https://doi.org/10.1002/smo.20240059.

[13] X. Yang, Y. Zhang, P. Sun, C. Peng, A review on renewable energy: conversion and utilization of biomass, Smart Mol. 2 (4) (2024) e20240019, https://doi.org/10.1002/smo.20240019.

[14] J. Caro, D. Albrecht, M. Noack, Why is it so extremely difficult to prepare shape-selective Al-rich zeolite membranes like LTA and FAU for gas separation, Sep. Purif. Technol. 66 (1) (2009) 143–147, https://doi.org/10.1016/j.seppur.2008.11.009.

[15] S. Yu, S. Kwon, K. Na, Synthesis of LTA zeolites with controlled crystal sizes by variation of synthetic parameters: effect of Na+ concentration, aging time, and hydrothermal conditions, J. Sol. Gel Sci. Technol. 98 (2) (2018) 411–421, https://doi.org/10.1007/s10971-018-4850-4.

[16] X. Zhang, D. Tong, W. Jia, D. Tang, X. Li, R. Yang, Studies on room-temperature synthesis of zeolite NaA, Mater. Res. Bull. 52 (2014) 96–102, https://doi.org/10.1016/j.materresbull.2014.01.008.

[17] S. Aguado, J. Gascón, J.C. Jansen, F. Kapteijn, Continuous synthesis of NaA zeolite membranes, Microporous Mesoporous Mater. 120 (1-2) (2009) 170–176, https://doi.org/10.1016/j.micromeso.2008.08.062.

[18] X. Gao, B. Gao, H. Liu, C. Zhang, Y. Zhang, J. Jiang, X. Gu, Fabrication of stainless steel hollow fiber supported NaA zeolite membrane by self-assembly of submicron seeds, Sep. Purif. Technol. 234 (2020) 116121, https://doi.org/10.1016/j.seppur.2019.116121.

[19] M. Zhou, H. Jonas, Assembly of oriented iron oxide and zeolite crystals via biopolymer films, J. Mater. Chem. 22 (47) (2012) 24877, https://doi.org/10.1039/c2jm35068h.

[20] Q. Wang, N. Li, B. Bolto, M. Hoang, Z. Xie, Desalination by pervaporation: a review, Desalination 387 (2016) 46–60, https://doi.org/10.1016/j.desal.2016.02.036.

[21] X. Xu, D. Nikolaeva, Y. Hartanto, P. Luis, MOF-based membranes for pervaporation, Sep. Purif. Technol. 278 (2021) 119233, https://doi.org/10.1016/j.seppur.2021.119233.

[22] X. Cheng, F. Pan, M. Wang, W. Li, Y. Song, G. Liu, H. Yang, B. Gao, H. Wu, Z. Jiang, Hybrid membranes for pervaporation separations, J. Membr. Sci. 541 (2017) 329–346, https://doi.org/10.1016/j.memsci.2017.07.009.

[23] T. Gui, F. Zhang, Y. Li, X. Cui, X. Wu, M. Zhu, N. Hu, X. Chen, H. Kita, M. Kondo, Scale-up of NaA zeolite membranes using reusable stainless steel tubes for dehydration in an industrial plant, J. Membr. Sci. 583 (2019) 180–189, https://doi.org/10.1016/j.memsci.2019.04.046.

[24] A. Huang, W. Yang, J. Liu, Synthesis and pervaporation properties of NaA zeolite membranes prepared with vacuum-assisted method, Sep. Purif. Technol. 56 (2) (2007) 158–167, https://doi.org/10.1016/j.seppur.2007.01.020.

[25] L. Wang, J. Yang, J. Wang, W. Raza, G. Liu, J. Lu, Y. Zhang, Microwave synthesis of NaA zeolite membranes on coarse macroporous α-Al2O3 tubes for desalination, Microporous Mesoporous Mater. 306 (2020) 110360, https://doi.org/10.1016/j.micromeso.2020.110360.

[26] N. Ma, Z. Zhan, Z. Wang, Manipulation of the surface microstructure and its effects on the flux of NaA zeolite membranes in pervaporation, Microporous Mesoporous Mater. 235 (2016) 100–106, https://doi.org/10.1016/j.micromeso.2016.08.006.

[27] Z. Yang, Y. Liu, C. Yu, X. Gu, N. Xu, Ball-milled NaA zeolite seeds with submicron size for growth of NaA zeolite membranes, J. Membr. Sci. 392–393 (2012) 18–28, https://doi.org/10.1016/j.memsci.2011.11.036.

[28] C. Xu, C. Zhou, S. Wang, A. Huang, Copper-exchanged LTA zeolite membranes with enhanced water flux for ethanol dehydration, Chin. Chem. Lett. 30 (6) (2019) 1204–1206, https://doi.org/10.1016/j.cclet.2019.01.016.

[29] F. Chen, Y. Li, A. Huang, Facile preparation of compact LTA molecular sieve membranes on polyethyleneimine modified substrates, Chin. Chem. Lett. 32 (3) (2021) 1086–1088, https://doi.org/10.1016/j.cclet.2020.07.047.

[30] Y. Li, J. Liu, W. Yang, Formation mechanism of microwave synthesized LTA zeolite membranes, J. Membr. Sci. 281 (1) (2006) 646–657, https://doi.org/10.1016/j.memsci.2006.04.051.

[31] M.P. Pina, M. Arruebo, M. Felipe, F. Fleta, M.P. Bernal, J. Coronas, M. Menéndez, J. Santamaría, A semi-continuous method for the synthesis of NaA zeolite membranes on tubular supports, J. Membr. Sci. 244 (1) (2004) 141–150, https://doi.org/10.1016/j.memsci.2004.06.049.

[32] K. Sato, K. Aoki, K. Sugimoto, K. Izumi, S. Inoue, J. Saito, S. Ikeda, T. Nakane, Dehydrating performance of commercial LTA zeolite membranes and application to fuel grade bio-ethanol production by hybrid distillation/vapor permeation process, Microporous Mesoporous Mater. 115 (1) (2008) 184–188, https://doi.org/10.1016/j.micromeso.2007.10.053.

[33] R. Tanaka, Y. Ito, Y. Hasegawa, T. Higuchi, Synthesis of LTA zeolite membranes from metal alkoxides and examination of the pervaporation performance, Microporous Mesoporous Mater. 326 (2021) 111346, https://doi.org/10.1016/j.micromeso.2021.111346.

[34] H. Zhang, Q. Zheng, Z. Wang, A facile preparation of high flux NaA zeolite membranes by direct secondary growth of wet gel layer, Sep. Purif. Technol. 329 (2024) 125211, https://doi.org/10.1016/j.seppur.2023.125211.

[35] M. Noack, P. Kölsch, A. Dittmar, M. Stöhr, G. Georgi, M. Schneider, U. Dingerdissen, A. Feldhoff, J. Caro, Proof of the ISS-concept for LTA and FAU membranes and their characterization by extended gas permeation studies, Microporous Mesoporous Mater. 102 (1-3) (2007) 1–20, https://doi.org/10.1016/j.micromeso.2006.12.024.

[36] P. Yu, G. Yang, Y. Chai, L. Tosheva, C. Wang, H. Jiang, C. Liu, H. Guo, Self-limiting growth of thin dense LTA membranes boosts H2 gas separation performance, Chem. Eng. J. 479 (2024) 147629, https://doi.org/10.1016/j.cej.2023.147629.

[37] L. Li, S. Xu, Z. Liu, D. Wang, Insight into the growth mechanism of low-temperature synthesis of high-purity lithium slag-based zeolite A, Materials 17 (3) (2024) 568, https://doi.org/10.3390/ma17030568.

[38] F.Z. Charik, B. Achiou, A. Belgada, Z.C. Elidrissi, M. Ouammou, M. Rabiller-Baudry, S.A. Younssi, Optimal preparation of low-cost and high-permeation NaA zeolite membrane for effective ethanol dehydration, Microporous Mesoporous Mater. 344 (2022) 112229, https://doi.org/10.1016/j.micromeso.2022.112229.

[39] E. Pan, S. Kwon, Z. Jensen, M. Xie, R. Gómez-Bombarelli, M. Moliner, Y. Román-Leshkov, E. Olivetti, ZeoSyn: a comprehensive zeolite synthesis dataset enabling machine-learning rationalization of hydrothermal parameters, ACS Cent. Sci. 10 (3) (2024) 729–743, https://doi.org/10.1021/acscentsci.3c01615.

[40] L. Fortunato, H. Elcik, B. Blankert, N. Ghaffour, J. Vrouwenvelder, Textile dye wastewater treatment by direct contact membrane distillation: membrane performance and detailed fouling analysis, J. Membr. Sci. 636 (2021) 119552, https://doi.org/10.1016/j.memsci.2021.119552.

[41] F. Dastoorian, A. Salem, S. Salem, Role of amine-based fuel combination in conventional and microwave-assisted smoldering combustion for production of mesoporous hydroxyapatite with super adsorptive characteristics for separation of disperse dye, Microporous Mesoporous Mater. 330 (2022) 111576, https://doi.org/10.1016/j.micromeso.2021.111576.

[42] Q. Wang, C. Qian, C. Guo, N. Xu, Q. Liu, B. Wang, L. Fan, K. Hu, Pervaporation dehydration mechanism and performance of high-aluminum ZSM-5 zeolite membranes for organic solvents, Int. J. Mol. Sci. 25 (14) (2024) 7723, https://doi.org/10.3390/ijms25147723.

[43] R. Castro-Muñoz, G. Boczkaj, Pervaporation zeolite-based composite membranes for solvent separations, Molecules 26 (5) (2021) 1242, https://doi.org/10.3390/molecules26051242.

[44] S. Padinjarekutt, B. Sengupta, H. Li, K. Friedman, D. Behera, R. Lecaros, M. Yu, Synthesis of Na+-gated nanochannel membranes for the ammonia (NH3) separation, J. Membr. Sci. 674 (2023) 121512, https://doi.org/10.1016/j.memsci.2023.121512.

[45] N. Hijazi, A. Bavykina, I. Yarulina, T. Shoinkhorova, E.V. Ramos-Fernandez, J. Gascon, Chemical engineering of zeolites: alleviating transport limitations through hierarchical design and shaping, Chem. Soc. Rev. 54 (13) (2025) 6335–6384, https://doi.org/10.1039/D5CS00169B.

[46] O. Kwon, M. Kim, E. Choi, J.H. Bae, S. Yoo, J.C. Won, Y.H. Kim, J.H. Shin, J.S. Lee, D.W. Kim, High–aspect ratio zeolitic imidazolate framework (ZIF) nanoplates for hydrocarbon separation membranes, Sci. Adv. 8 (1) (2022), https://doi.org/10.1126/sciadv.abl6841 eabl6841.

[47] A. Mayoral, Q. Zhang, Y. Zhou, P. Chen, Y. Ma, T. Monji, P. Losch, W. Schmidt, F. Schüth, H. Hirao, J. Yu, O. Terasaki, Direct atomic-level imaging of zeolites: oxygen, sodium in Na-LTA and iron in Fe-MFI, Angew. Chem., Int. Ed. 59 (44) (2020) 19510–19517, https://doi.org/10.1002/anie.202006122.

[48] K. Ooe, T. Seki, K. Yoshida, Y. Kohno, Y. Ikuhara, N. Shibata, Direct imaging of local atomic structures in zeolite using optimum bright-field scanning transmission electron microscopy, Sci. Adv. 9 (31) (2023), https://doi.org/10.1126/sciadv.adf6865 eadf6865.

[49] M.K. Choudhary, R. Jain, J.D. Rimer, In situ imaging of two-dimensional surface growth reveals the prevalence and role of defects in zeolite crystallization, Proc. Natl. Acad. Sci. 117 (46) (2020) 28632–28639, https://doi.org/10.1073/pnas.2011806117.

[50] X. Wei, J. Zhang, W. Pan, B. Song, Y. Luo, Q. Liu, Z. Shi, X. Li, Z. Miao, Reusable saturated synthesis solutions for compact zeolite membranes, Microporous Mesoporous Mater. 376 (2024) 113180, https://doi.org/10.1016/j.micromeso.2024.113180.